



Removal of wood dyes from aqueous solutions by sorption on untreated pine (*Pinus radiata*) sawdust

Catarina H. Pimentel · M. Sonia Freire ·
Diego Gómez-Díaz · Julia González-Álvarez

Received: 26 October 2022 / Accepted: 10 March 2023
© The Author(s) 2023

Abstract In this work, the possibility of using untreated pine (*Pinus radiata*) sawdust as biosorbent for the removal of three wood dyes (blue, red and black) from aqueous solutions was investigated. The BET surface area of the material was $1.55 \pm 0.81 \text{ m}^2 \text{ g}^{-1}$ using N_2 at $-196 \text{ }^\circ\text{C}$ and $17.83 \pm 0.032 \text{ m}^2 \text{ g}^{-1}$ using CO_2 at $0 \text{ }^\circ\text{C}$. The point of zero charge was 4.8. In addition, the material was characterized before and after adsorption by surface analytical techniques. Assays were performed to analyze the stability of wood dyes with time and pH and also to estimate the pKa values. Batch adsorption experiments were performed and the influence of experimental parameters such as contact time (up to equilibrium), stirring rate (100 and 210 rpm), adsorbent dose ($2\text{--}10 \text{ g L}^{-1}$), pH (2–9) and initial dye concentration (5 and 300 mg L^{-1}) were studied. The optimum conditions were pH 2 and adsorbent dose of 6 g L^{-1} and the highest adsorption percentages achieved at 5 mg L^{-1} were: 100.0% for the blue, 99.7% for the black and 92.4% for the red. For 300 mg L^{-1} adsorption efficiency decreased

to 85.6, 57.0 and 63.8% for the blue, black and red ones, respectively. Kinetic data were best fitted to the pseudo-second order model, suggesting a chemisorption process. Freundlich and Dubinin-Radushkevich were the best isotherm models. Regeneration study showed that un-treated pine sawdust could be reused efficiently for red dye removal at least in up to four repeated adsorption–desorption cycles using NaOH as desorption agent.

Keywords Biomass · Pine sawdust · Wood dyes · Biosorption · Wastewaters · Chemisorption

Introduction

Synthetic dyes are essential resources used in industries like wood, paper, cosmetic, textile, etc. to color their products. It is estimated that there are more than 100,000 commercial dyes and about 350,000 tons are wasted every year (Şentürk and Yildiz 2020). The discharge of these dyes in wastewaters without treatment is of great concern for the environment and human health since it prevents photosynthesis by reducing light transmission and compromises the food chain transfer. In addition, the complex and stable chemical structure of the dyes tends to resist degradation when in contact with water, oxidizing agents, light, among others. On the other hand, dyes can cause functional disorders in the human body and their accumulation in some aquatic organisms carries the risk of toxic

Supplementary Information The online version contains supplementary material available at <https://doi.org/10.1007/s10570-023-05145-4>.

C. H. Pimentel · M. S. Freire · D. Gómez-Díaz ·
J. González-Álvarez (✉)
Department of Chemical Engineering, School
of Engineering, Universidade de Santiago de
Compostela, Rúa Lope Gómez de Marzoa s/n,
15782 Santiago de Compostela, Spain
e-mail: julia.gonzalez@usc.es

and carcinogenic products (Gemici et al. 2021; Chikri et al. 2020). Furthermore, water is an essential component for life and the earth's ecosystem and its protection and prevention of contamination are crucial.

There are a variety of techniques that have been studied for the removal of dyes from wastewaters, such as chemical oxidation, ion exchange, photocatalysis, biodegradation, chemical coagulation, electrolysis, precipitation, membrane separation, and flotation. However, most of these techniques involve disadvantages such as the high cost, the generation of huge amounts of concentration sludge, a reduced efficiency, and sensitive operating conditions (Can 2015; Al-Kadhi 2020; Chandarana et al. 2021). An efficient technique to remove dyes from wastewaters should be able to eliminate large amounts of dye in a short period of time without causing secondary pollution (Mashabi et al. 2022).

The adsorption technique being cost-efficient and with a simple design and operation has been revealed as one of the most effective processes for dye removal (Kumar et al. 2018; Elwakeel et al. 2017). A wide range of adsorbents have been used for dye removal from aqueous solutions. Activated carbons have been the most applied ones mainly due to their high surface area and porosity, however, their high cost and their regeneration difficulty have promoted the research on low-cost adsorbents (Ighalo et al. 2022; Philippou et al. 2021). Numerous biowastes such as grapefruit peel, canola hull, pine cone, pine sawdust, peanut husk and rice hull have been pointed out as promising biosorbents due to the lack of hazardous by-product formation, eco-friendliness, cost-effectiveness, flexibility regarding operating conditions and good surface characteristics (Aragaw and Bogale 2021).

Pine trees of various species are present in huge amounts around the world. They are among the most commercially important trees highly valued by industry (Özdemir 2019). In northwest Spain, monterrey pine (*Pinus radiata*) and maritime pine (*Pinus pinaster*) are important natural resources and together with eucalyptus the most used in productive stands (Ogana et al. 2020). Pine sawdust is available as a residue from the wood industry and inherent activities and by using it as an adsorbent, wood waste which are improperly disposed on the environment could be reduced (Bortoluz et al. 2020). Previous studies revealed that the functional groups present in this material like carboxyl, phenolic or hydroxyl enhance the adsorption process

through mechanisms such as complexation, hydrogen bonding, ion exchange, etc. (Aragaw and Bogale 2021; Şentürk and Yildiz 2020). Further, pine sawdust from species like *Pinus duragensis*, *Pinus resinosa*, and *Pinus tabulaeformis* have been previously investigated for dyes removal such as acid yellow and methylene blue and revealed promising results (Can 2015; Salazar-Rabago et al. 2017; Sahmoune and Yeddou 2016). However, it has been found that the wood species affects significantly the adsorption capacity (Salazar-Rabago et al. 2017). Additionally, some studies have reported the need for an acid or base pretreatment or an extensive washing to improve the adsorption efficiency (Şentürk and Yildiz 2020; Bortoluz et al. 2020; Islam et al. 2018) while others obtained a positive outcome without any previous treatment which is a simpler and more profitable alternative (Al-Kadhi 2020; Akhouairi et al. 2019). The conversion of biomass into products of high added value is a significant contribution to the circular economy and to the concept of green chemistry. Therefore, at present, the search for biosorbents for dyes removal is attracting attention which highlights the importance of the present study (Philippou et al. 2021; Aragaw and Bogale 2021).

To the best of authors' knowledge, no studies have been conducted on the removal of wood dyes from aqueous solutions by pine (*Pinus radiata*) sawdust. Therefore, in the present study, pine (*Pinus radiata*) sawdust, received from a sawmill without any pretreatment, was directly used as an alternative, cost-effective and environmentally friendly adsorbent for the removal of three industrial acid wood dyes (blue, red and black) from aqueous solutions. Batch experiments were performed to evaluate the influence of various operational conditions such as stirring rate, adsorbent dose, pH, contact time and initial dye concentration. The kinetics of the adsorption process using pseudo-first, -second and intraparticle diffusion models was studied and the Langmuir, Freundlich, Temkin and Dubinin-Radushkevich isotherms were used to fit the equilibrium data.

Materials and methods

Adsorbent preparation

Pine (*Pinus radiata*) sawdust (PS) was provided by a regional sawmill (Lugo, Spain). It was air-dried

till equilibrium and the corresponding moisture content (11.61 wt%, on wet basis) was determined using an Infrared moisture determination balance (Sartorius MA30). Then, PS was sieved using a Ro-Tap type electrical sieve shaker (FTL-0200). The fraction between 0.5 and 1 mm was selected, stored in a plastic container, and used directly for adsorption experiments. Before adsorption experiments and to assure that PS does not release colored components that could interfere adsorption measurements, PS was kept in water (5 g L^{-1}) for 24 h in an Unitronic orbital C shaker (Selecta) at 100 rpm, $25 \text{ }^\circ\text{C}$ and pH 2, natural (5.1) and 12. Color release was observed at pH 12 whereby this pH was excluded for adsorption experiments.

Adsorbent characterization

The surface area, pore volume and structural properties of PS were determined by adsorption/desorption of N_2 at $-196 \text{ }^\circ\text{C}$ using an ASAP 2020 surface area analyzer (Micromeritics). This characterization was completed by adsorption experiments with CO_2 at $0 \text{ }^\circ\text{C}$ with the same equipment in order to analyze the ultramicroporosity of the material. Previously, the samples were dried under vacuum at $50 \text{ }^\circ\text{C}$ for 72 h and then degassed under vacuum at $300 \text{ }^\circ\text{C}$ for 1 h. Brunauer-Emmet-Teller (BET) equation was used to determine surface areas and Barrett-Joyner-Halenda (BJH) desorption isotherm to determine the pore volume and pore size distribution. A relative pressure of 0.99 was used to determine the total pore volume and to estimate micropore volume based on mesopores volume (from the BJH equation). PS was analyzed by scanning electron microscope coupled with EDX (ZEISS EVO LS 15 microscope) to study its morphological features and to determine its elemental composition before adsorption. For SEM analysis, PS samples were covered with a thin layer of iridium. The pH of the point of zero charge (pH_{PZC}) for PS was evaluated according to the method described in Şentürk and Yildiz (2020), although slightly modified. Thus, 0.2 g of PS were put in contact with 50 mL of a 0.01 M NaCl solution at 200 rpm for 48 h to assure equilibrium (Nordine et al. 2016).

Dye characterizations

Acid wood dyes were used: Blue for wood AGN-270%, Red for wood GRA-200%, and Black Hispalian M-RN-140%. Dye solutions were prepared by dilution of a stock aqueous solution of 500 mg L^{-1} with distilled water. The elemental composition of the dyes was determined by EDX. To study dye stability, 50 mL of dye solution (25 mg L^{-1}) at natural pH (5.1, 6.0 and 6.2 for blue, black and red dyes, respectively) and at pH 2 were placed in a hydro shaking water bath (H2O SOW-LAUDA) at 210 rpm and $25 \text{ }^\circ\text{C}$. For predefined times (from 30 min to 96 h), the visible absorption spectra of the samples were recorded by UV/VIS spectroscopy (V-630, Jasco).

The determination of the dissociation constant (pK_a) was performed using two different techniques. Regarding the red dye that presents a color shift with pH changes, pK_a was determined using the UV/VIS spectroscopy method by measuring the absorption wavelength (V-630, Jasco) of a 10 mg L^{-1} solution at pH values from 1.5 to 12.5 following the method proposed by De Meyer et al. (2014). For the blue and black dyes, pK_a values were determined by potentiometric titration. An aqueous solution of each dye (10 mg L^{-1}) was titrated potentiometrically at $25 \text{ }^\circ\text{C}$ under continuous stirring by adding small aliquots (0.05 mL) of 0.05 M NaOH up to pH 11. For weak acids, the pH could be calculated as follows:

$$\text{pH} = \text{pK}_a + \log\left[\frac{[\text{A}^-]}{[\text{HA}]}\right] \quad (1)$$

where $[\text{A}^-]$ is the conjugate base and $[\text{HA}]$ the weak acid. The half-neutralization point occurs when $[\text{A}^-]$ is equal to $[\text{HA}]$ that corresponds to $\text{pH} = \text{pK}_a$ (Zafar et al. 2014; Kantar et al. 2015).

Adsorption experiments

In a first stage, experiments were performed at 100 rpm in an Unitronic orbital C shaker (Selecta). For this, PS was mixed with a 5 mg L^{-1} dye aqueous solution at adsorbent doses of 5 or 10 g L^{-1} , natural pH (5.1, 6.0 and 6.2 for blue, black and red dyes, respectively) and $25 \text{ }^\circ\text{C}$. In a second stage, to evaluate the effect of the agitation speed on adsorption efficiency experiments were performed at 210 rpm and adsorbent dose of 10 g L^{-1} at the same previous

conditions. Finally, the influence of other variables was also studied at 210 rpm: initial pH (2–9), adsorbent dose (2, 6 and 10 g L⁻¹) and initial dye concentration (5 and 300 mg L⁻¹). At predefined times, samples were removed and centrifuged for 15 min at 4000 rpm. Dye concentration was determined by measuring the absorbance of the supernatant at the maximum dye wavelength, λ_{\max} , using an UV/VIS spectrophotometer (V-630, Jasco). Dye removal efficiency was calculated as the percentage of dye adsorbed (Eq. 2). The adsorption capacity was calculated as the amount of dye adsorbed per mass unit of PS (Eq. 3).

$$\text{Adsorption (\%)} = (C_0 - C)/C_0 \times 100 \quad (2)$$

$$q(\text{mg g}^{-1}) = (C_0 - C)V/m \quad (3)$$

where C_0 and C are the initial and residual dye concentrations (mg L⁻¹), q is the adsorption capacity (mg g⁻¹), V is the volume of the dye solution (L) and m is the dry mass of adsorbent used (g).

SEM-EDX was conducted to characterize the PS samples after the adsorption process as explained above.

Kinetic models were applied to explain the dye adsorption process and examine the mechanism of the interactions:

- Pseudo-First Order

$$\log(q_e - q_t) = \log q_e - k_1 t / 2.303 \quad (4)$$

where q_t and q_e are the amounts of dye adsorbed (mg g⁻¹) at time t (min) and at equilibrium, respectively, and k_1 represents the first-order rate constant (min⁻¹).

- Pseudo-Second Order

$$t/q_t = (1/k_2 q_e^2) + t/q_e \quad (5)$$

where k_2 (g mg⁻¹ min⁻¹) is the pseudo-second-order rate constant (Ho and McKay 1999).

- Intra-particle Diffusion

$$q_t = k_{id} t^{1/2} + I \quad (6)$$

where I is the intercept and k_{id} is the rate constant of intra-particle diffusion (mg g⁻¹ min^{-1/2}) (Weber et al. 1963).

The adsorption equilibrium was studied using the operational conditions selected in the previous studies. PS (6 g L⁻¹) was mixed with a dye aqueous solution (initial concentrations varied between 5 and 300 mg L⁻¹) at pH 2 and 25 °C for 4 days for blue and red to assure the equilibrium and 12 h for black also to guarantee the stability. The equilibrium data were analyzed by the Freundlich (Eq. 7), Langmuir (Eq. 8), Temkin (Eq. 9) and Dubinin-Radushkevich (D-R) (Eq. 10) isotherm models:

$$q_e = k_F C_e^{1/n} \quad (7)$$

$$q_e = \frac{q_{\max} k_L C_e}{1 + k_L C_e} \quad (8)$$

$$q_e = B(\ln K_T C_e) \quad (9)$$

$$q_e = q_{m,D} \exp(-K_{DR} \epsilon^2) \quad (10)$$

where q_e and q_{\max} are the amount of dye adsorbed at equilibrium and the maximum adsorption capacity (mg g⁻¹); k_F [mg g⁻¹ (L mg⁻¹)^{-1/n}] and k_L (L mg⁻¹) are the Freundlich and Langmuir constants; C_e is the equilibrium dye concentration (mg L⁻¹); n represents the intensity of the adsorption (Langmuir 1918; Freundlich 1907); K_T is the equilibrium binding constant (L mg⁻¹); B is related to the adsorption heat (J mol⁻¹) (Chandarana et al. 2020); ϵ is equal to $RT \ln(1 + 1/C_e)$; $q_{m,D}$ is the theoretical monolayer saturation capacity (mol g⁻¹); and K_{DR} is the constant of the adsorption energy (mol² kJ⁻²) which is related to the mean adsorption energy, E , equal to $1/\sqrt{2K_{DR}}$ (kJ mol⁻¹) (Collins et al. 2019; Özdemir 2019) Langmuir model can also be characterized by another parameter, the adsorption rate (R_L), that can be determined using Eq. (11). R_L indicates if the adsorption process is irreversible, linear or favorable according to the R_L value, $R_L = 0$, $R_L = 1$ and $0 < R_L < 1$, respectively (Al-Kadhi 2020, Şentürk and Yildiz 2020)

$$R_L = \frac{1}{1 + k_L C_0} \quad (11)$$

Desorption and regeneration of the adsorbent

Batch desorption experiments were conducted to evaluate the possibility of reusing *Pinus radiata* sawdust after performing an adsorption experiment using an adsorbent dose of 10 g L^{-1} , pH 2, a dye concentration of 300 mg L^{-1} and a contact time of 4 days for the blue and red dyes and 12 h for the black dye. Then, the loaded adsorbent was filtered and dried at $105 \text{ }^\circ\text{C}$ for 24 h. Two desorption agents were selected, namely, hydrochloric acid 0.1 M and sodium hydroxide 0.1 M (Bortoluz et al. 2020; Mashkoor et al. 2018). In this way, 0.5 g of loaded PS were put in contact with 10 mL of the selected desorption agent and agitated at 350 rpm on the orbital shaker VWR (Cienytech) at $25 \text{ }^\circ\text{C}$ for 4 h. Then the suspension was filtered and the solid washed with distilled water until neutral pH. Before filtration, the residual dye concentration in the solution was measured as indicated before, and the desorption percentage (%Desorption) was calculated by Eq. 12:

$$\%Desorption = m_{des}/m_{rem} \times 100 \quad (12)$$

$$m_{rem} = m_{retained} + m_{adsycle} \quad (13)$$

where, m_{des} is the amount of dye desorbed (mg), m_{rem} is the mass of dye that remained adsorbed on the PS after each adsorption/desorption cycle (mg), $m_{retained}$ is the mass retained after the previous desorption cycle (mg) and $m_{adsycle}$ is the amount of dye adsorbed in each adsorption cycle (mg). The reusability of PS was studied by carrying out four repeated adsorption–desorption cycles and each cycle was evaluated by the percentages of dye adsorption and desorption.

Results and discussion

Adsorbent characterization

In this study gas sorption isotherms were performed for N_2 at $-196 \text{ }^\circ\text{C}$ and CO_2 at $0 \text{ }^\circ\text{C}$ to examine the surface area and pore structure of PS. The nitrogen adsorption–desorption plot is shown in Fig. 1.

The N_2 isotherm is mainly type II which is typical of macroporous materials with heterogeneous surface

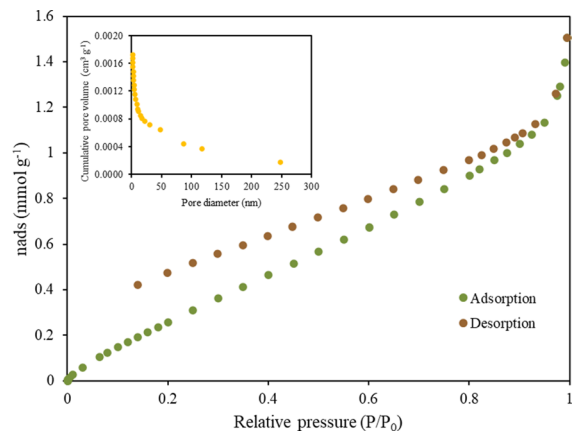


Fig. 1 Nitrogen adsorption–desorption cycle at $-196 \text{ }^\circ\text{C}$ on PS and BJH pore size distribution

according to the IUPAC classification (Rouquerol et al. 2014). Physical adsorption on macroporous adsorbents leads to unrestricted monolayer–multilayer adsorption. However, the initial behavior of N_2 adsorption capacity at low pressure corresponds to a type III isotherm, suggesting that the material also contains micro and mesopores that will lead to the formation of multiple layers with increasing relative pressure. The hysteresis between the adsorption and desorption curves at high relative pressures could be associated with the filling and emptying of mesopores by capillary condensation. The asymptotic behavior which occurs at relative pressures approaching one, suggests a significant amount of macropores (Lorenz et al. 2019). A similar behavior has been reported by Jaouadi (2021) for pinewood sawdust. The PS BET surface area, total pore volume and mean pore diameter for N_2 were, respectively, $1.55 \pm 0.81 \text{ m}^2 \text{ g}^{-1}$, $1.94 \times 10^{-3} \text{ cm}^3 \text{ g}^{-1}$ and 5.15 nm . According to the pore size distribution (Fig. 1) that indicates that the major pore size is in the range between 2 and 50 nm, PS can be categorized as a mesoporous material since the average pore diameter was between 2 and 50 nm according to the pore’s IUPAC classification (Rouquerol et al. 2014). Similar values have been reported for pine and durian (*Durio zibethinus*) wood sawdust (Chowdhury et al. 2016; Jaouadi 2021). Previous studies demonstrated that N_2 adsorption–desorption isotherm could have some limitations for ultra-microporous materials as N_2 cannot access into the micropores (Kim et al. 2016). To obtain a greater insight into the porosity of PS, and due to the

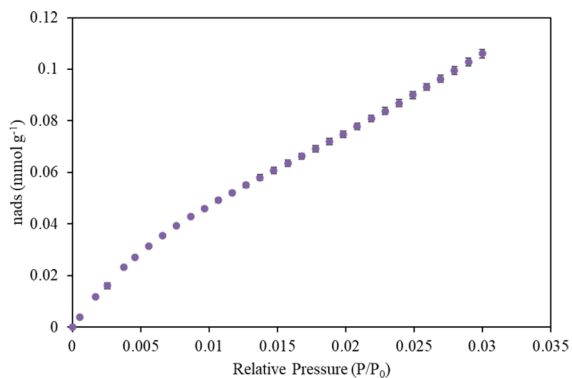


Fig. 2 CO₂ adsorption isotherm at 0 °C on PS

hysteresis cycle, which suggests microporosity, CO₂ adsorption isotherm was studied. Figure 2 shows the CO₂ adsorption isotherm recorded up to a relative pressure of 0.03 at 0 °C.

By the results obtained, PS revealed a higher BET surface area with CO₂ adsorption of $17.83 \pm 0.032 \text{ m}^2 \text{ g}^{-1}$ suggesting that microporosity could play an important role in adsorbate accessibility.

The morphology of the PS surface was analyzed by SEM. The images of the biosorbent before the adsorption process are shown in Fig. 3.

As can be seen in Fig. 3a with 500 magnifications, PS presented a multi-layer surface with a tubular structure (Semerjian 2018). Figure 3b and c with 1000 and 5000 magnifications respectively,

revealed a heterogeneous and fibrillar structure with pores which can favor the adsorption process. Similar characteristics were found in previous studies for *Pinus elliottii*, *Tectona grandis* and *Pinus halepensis* sawdust (Akhouairi et al. 2019; Semerjian 2018; Mashkoo et al. 2018).

The elemental composition of PS is shown in Table 1. The results indicated that carbon and oxygen are the main components due to the organic nature of the material and presented traces of Al that could result from the material used to cut in the sawmill. In addition, pine sawdust contained only a small amount of Cu, K, Ca and Mg which indicates that the content of metals on the surface were negligible.

The relationship between pH and p*H*_{PZC} plays a key role in understanding the adsorption process since pH affects the surface charge of the adsorbent, the degree of ionization, and in turn, the binding specificity of the adsorbate. The point of zero charge of PS is 4.8 (Fig. S1), indicating that when the pH is lower than p*H*_{PZC} the PS surface is positively charged and negatively charged when it is higher than p*H*_{PZC}. When pH is less than p*H*_{PZC} the sawdust will adsorb anionic dyes and when pH is higher than p*H*_{PZC} the adsorbent will adsorb cationic dyes (Ratnamala et al. 2016). Acid wood dyes are negatively charged, so it is probable that a positively charged PS surface leads to increased adsorption of acid dye anions.

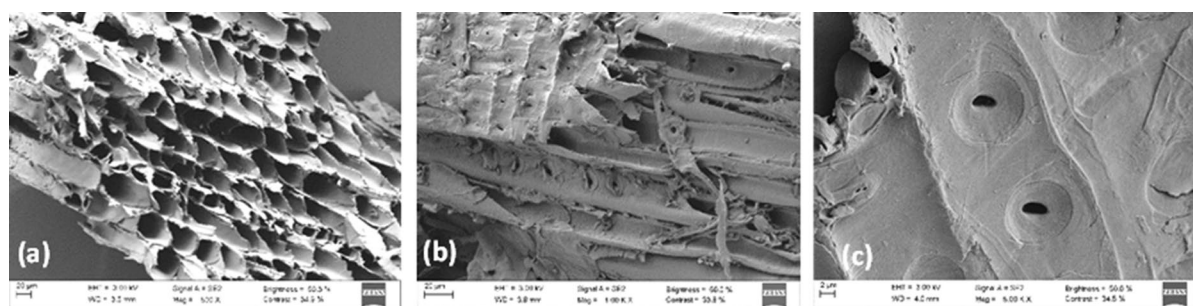


Fig. 3 SEM images of pine sawdust before adsorption **a** 500, **b** 1000 and **c** 5000 magnifications

Table 1 Elemental composition of pine sawdust

	wt%						
PS	C	O	Al	Cu	K	Ca	Mg
	58.6 ± 0.1	38.8 ± 0.1	2.0 ± 0.0	0.3 ± 0.0	0.1 ± 0.0	0.1 ± 0.0	0.1 ± 0.0

Dyes characterization

The elemental composition of the dyes was analyzed by EDX and is shown in Table 2. The results indicated that the main component is carbon together with a considerable oxygen percentage, especially for the red dye. For the black dye, the presence of chromium and the high sulfur content stand out. Thus, considerable differences were found among dyes both in terms of the components present and their percentage contribution.

Dye stability as a function of pH at 25 mg L⁻¹ was studied (Figs. S2a-f). From the spectral scans, the maximum wavelength in the visible region to consider for the stability study were 602 nm, 506 nm and 572 nm for the blue, red and black dyes, respectively. For the blue and red dyes, either for natural (Figs. S2a, S2c) or acid pH (Figs. S2b, S2d), there were no significant changes in the absorbance values for 4 days, which demonstrates their stability. For the black dye, the stability was also verified at natural pH (Fig. S2e). Otherwise, at acid pH a decrease on dye absorbance of about 10% occurred up to 12 h being more evident (30%) at 4 days. Simultaneously, there was a shift of the maximum wavelength with the consequent loss of stability after 12 h (Fig. S2f). Thus, for the black dye, further experiments were only performed up to 12 h assuring the stability region.

Acid dissociation constant (pKa) is an important parameter to better understand the behavior of chemical substances. Changing the availability of protons or the acidity of the medium the equilibrium changes which provides the possibility of measuring the capacity of protons release or dissociation of a site. The pKa could be described as the pH at which the protonated and deprotonated forms are equal. Thus, the site will be more deprotonated or protonated as the pH is higher or lower than pKa, respectively (Zafar et al. 2014).

Firstly, the visible spectrum of the red dye at different pH values was obtained from UV/VIS spectroscopy (Fig. S3). It can be observed that the color changes from red to orange at pH higher than 10 which corresponds with a shift of λ_{\max} from 506 to 483 nm (Fig. S3a). A change in acidity that leads to color changes is usually due to the presence of a chromophore close to the ionization site of the molecule (Reijenga et al. 2013). The pKa was estimated from the crossing point in Fig. S3b as 10.6, through the measure of the absorbance at the two maximum wavelengths previously determined at each pH value.

To estimate the pKa values of the blue and black dyes in aqueous solution, direct micro-potentiometry titration was performed with NaOH as a strong base as commented before. The pH variation for these dyes with the addition of NaOH is shown in Fig. S4. It can be observed that from 0 to 60 μ L the pH significantly increases from 6 to 10 and then it stabilizes forming a buffer zone used to calculate the pKa as the pH of the half neutralization point. It was found to be 10.4 for the blue dye and 10.3 for the black one.

It can be seen that there are no significant differences among the pKa values of the red, blue and black dyes which would be related with their molecular structures and functional groups, and since the lower the pKa the stronger the acidity, the dyes used in this study could be classified as weak acids (Zafar et al. 2014; Kantar et al. 2015; Schaffer and Licha 2014).

Adsorption experiments

Effect of adsorbent dose and agitation speed at natural pH

Adsorption experiments were started at the natural pH of the dyes solutions and Fig. 4a shows the results obtained for the adsorption efficiency versus time for the blue, red, and black dyes at two adsorbent doses (5

Table 2 Elemental composition of wood dyes

Dye	wt%											
	C	O	N	S	Na	Cl	Br	Cu	P	Cr	Mg	
Blue	62.1±0.1	18.4±0.1	7.2±0.1	6.7±0.0	4.8±0.0	0.4±0.0	0.2±0.0	0.1±0.0	–	–	–	
Red	49.7±0.1	28.3±0.1	3.4±0.1	7.1±0.0	10.1±0.0	0.9±0.0	–	0.1±0.0	0.4±0.0	–	–	
Black	27.5±0.2	18.4±0.1	–	21.3±0.1	11.1±0.1	–	–	1.6±0.1	–	20.0±0.1	0.1±0.0	

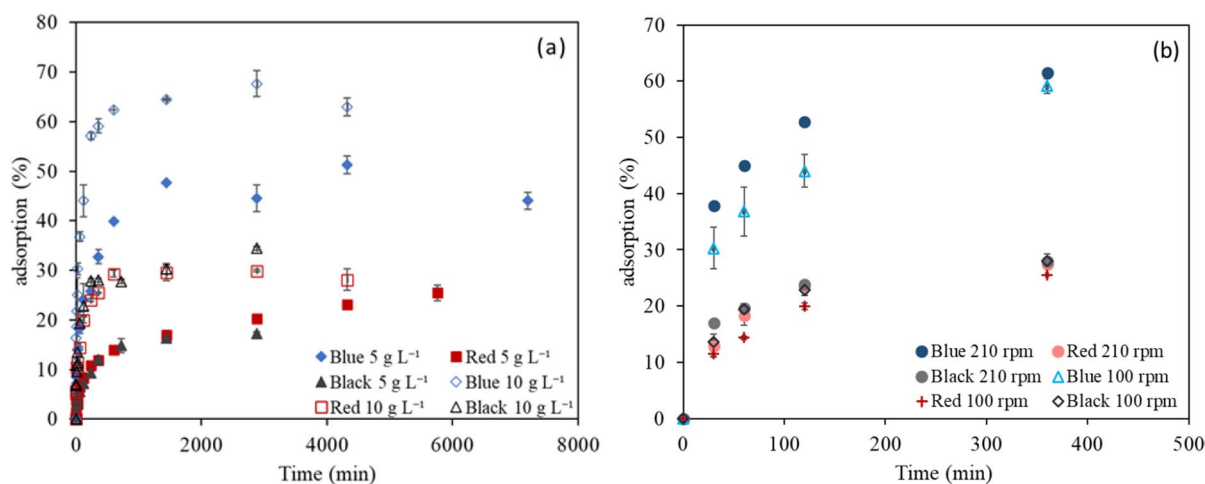


Fig. 4 Adsorption efficiency versus time for blue, red and black dyes at the natural pH **a** adsorbent dose 5 or 10 g L⁻¹, initial dye concentration 5 mg L⁻¹, temperature 25 °C, agita-

tion speed 100 rpm, **b** agitation speed 100 or 210 rpm, adsorbent dose 10 g L⁻¹, initial dye concentration 5 mg L⁻¹, temperature 25 °C

Table 3 Equilibrium removal efficiency and adsorption capacity for blue, red and black wood dyes onto pine sawdust

Adsorbent dose	Blue	Red	Black
(g L ⁻¹)	<i>Equilibrium dye adsorption efficiency (%)</i>		
5	51.30 ± 1.83	25.47 ± 1.54	17.25 ± 0.37
10	67.67 ± 2.46	29.93 ± 0.27	34.46 ± 0.34
	<i>Equilibrium adsorption capacity (mg g⁻¹)</i>		
5	0.51 ± 0.02	0.28 ± 0.02	0.18 ± 0.00
10	0.37 ± 0.03	0.16 ± 0.00	0.18 ± 0.00

and 10 g L⁻¹), initial dye concentration of 5 mg L⁻¹, 100 rpm and 25 °C. As can be seen, the adsorption proceeds in two stages. A fast first stage is followed by a slower one until equilibrium is reached. At the initial phase, the sawdust presents a more available and porous surface, with the presence of mesopores, which favors the rapid adsorption of the dye. As the adsorption progresses the surface becomes progressively saturated with the consequent decrease in the number of sorption sites on the PS and the adsorption becomes slower (Al-Kadhi 2020).

The time necessary to reach equilibrium was 72 h at 5 g L⁻¹ and 48 h at 10 g L⁻¹ for the blue dye, 96 h at 5 g L⁻¹ and 48 h at 10 g L⁻¹ for the red one, and 48 h for the black one at both adsorbent doses. The maximum adsorption efficiency was attained for the blue dye at both adsorbent doses (Table 3) which

can be related to the lower natural pH of this dye (5.1) in comparison with those of the black (6.0) and the red (6.2) ones. At pH far above the p*H*_{PZC} the surface might be more negatively charged, and this could lead to electrostatic repulsion and, consequently, to a lower amount of dye adsorbed. Previous studies with pine sawdust also demonstrated that for acid dyes, adsorption improved at lower pH (Can 2015; Akhouairi et al. 2019; Özacar and Şengil 2005).

Table 3 shows the influence of the adsorbent dose on the equilibrium adsorption efficiency and capacity. The adsorption efficiency increased when increasing the adsorbent dose from 5 to 10 g L⁻¹, but more remarkably for the blue and black dyes. This can be explained by the increase in the number of available adsorption sites and enhanced surface area due to larger adsorbent dose. Regarding the equilibrium adsorption capacity (*q*_{max}), it decreased with increasing the adsorbent dose, except for the black dye which does not change.

To investigate the effect of the agitation speed, kinetic experiments were conducted at 210 rpm. Figure 4b shows that the first stage gets faster when agitation speed is increased even though equilibrium conditions do not change significantly. Consequently, all other experiments were carried out at 210 rpm.

Effect of pH on dye adsorption

The pH is a significant parameter that influences the interaction between adsorbate and adsorbent depending on the ionization degree and surface characteristics (Şentürk and Yildiz 2020). Adsorption experiments were performed at different contact times assuring the stability of the dyes (Fig. S2), for an adsorbent dose of 10 g L^{-1} and initial dye concentration of 5 mg L^{-1} , at different pH values ranging from 2 to 9 and the results obtained are shown in Fig. 5. From these results it can be concluded, as mentioned previously, that pH has a significant effect on dye removal efficiency.

The maximum dye removal efficiency was obtained at pH 2 and it was 100.0% for the blue dye, 95.1% for the red dye and 85.5% for the black one. When pH increased from 2 to 9, adsorption efficiency rapidly decreased to 50.5%, 34.2% and 27.7% for the blue, red and black dyes, respectively. It is possible to explain the nature of possible charge-driven interactions based on the pH_{PZC} of the adsorbent and the pK_a of the adsorbate (Kah et al. 2017). Depending on the dye molecular structure and according to the estimated values of the pK_a (10.6, 10.4 and 10.3 for the red, blue and black dyes, respectively), at acid pH below the pK_a , the adsorbate could be protonated to the neutral form which can lead to interactions between the functional groups (Lewis acid–base, π – π

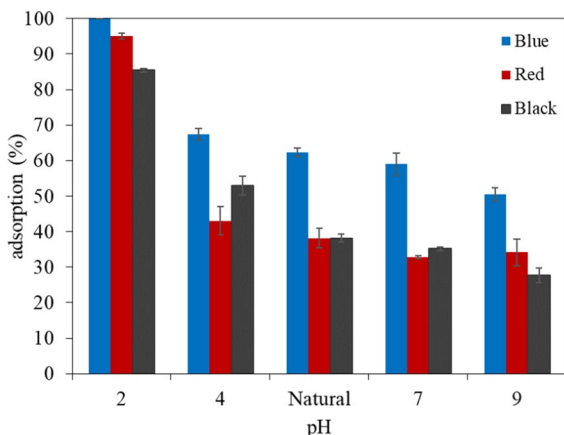


Fig. 5 Effect of pH on adsorption of blue, red and black wood dyes by PS (natural pH 5.1, 6.2 and 5.8 for blue, red and black, respectively; initial dye concentration 5 mg L^{-1} ; adsorbent dose 10 g L^{-1} ; contact time 24 h for blue, 48 h for red and 12 h for black; temperature $25 \text{ }^\circ\text{C}$; agitation speed 210 rpm)

bond, hydrophobic effect and H-bond). Moreover, since the PS surface is positively charged when the pH is below the pH_{PZC} (4.8) with a high concentration of H^+ in solution, acid dye anions are expected to interact electrostatically and to increase the adsorption capacity (Can 2015; Kah et al. 2017; Konicki et al. 2013). Other studies also reported that the optimum pH is usually around 2–4 since as pH decreases, the protonation of amine groups increases (Elwakeel 2010). These results demonstrated that for all dyes a better removal efficiency is attained at pH 2 instead of natural pH and subsequent experiments were conducted at acid pH.

Adsorption experiments at acid pH

Dye adsorption on PS at the pH selected ($\text{pH}=2$) was analyzed depending on contact time and adsorbent dose to determine the equilibrium time and the optimal adsorbent dose. The results are shown in Fig. 6.

The behavior of the adsorption process did not differ from the aforementioned for natural pH. The total removal of the blue dye was achieved at all adsorbent doses, however the equilibrium time increased from 30 min to 6 and 48 h when the PS dose decreased from 10 to 6 and 2 g L^{-1} , respectively. Regarding the red dye from 10 to 6 g L^{-1} there was no change in the equilibrium time (18 h) but a slight difference on removal efficiency from 98.3% to 92.4% occurred. Conversely, for 2 g L^{-1} there was a significant increase in the equilibrium time to 48 h and also a decrease in the removal efficiency (86.2%). In the case of black dye, to guarantee the stability, the study was performed for 12 h, and from 10 to 6 g L^{-1} both equilibrium time (2 h) and removal efficiency (99%) were maintained but the adsorption efficiency decreased to approximately 80% and the equilibrium time increased to 12 h when the adsorbent dose was reduced to 2 g L^{-1} . Consequently, it can be concluded that for all dyes at pH 2 and low concentration the optimum adsorbent dose is 6 g L^{-1} . This improvement on the adsorption process compared to the previous results could be described by the effect of ionic interaction due to the low pH value (Chikri et al. 2020; Özacar and Şengil 2005).

To overcome the diffusible mass transfer resistance in the adsorption process between the aqueous and solid phases, initial dye concentration is an important variable to be assessed which provides an important

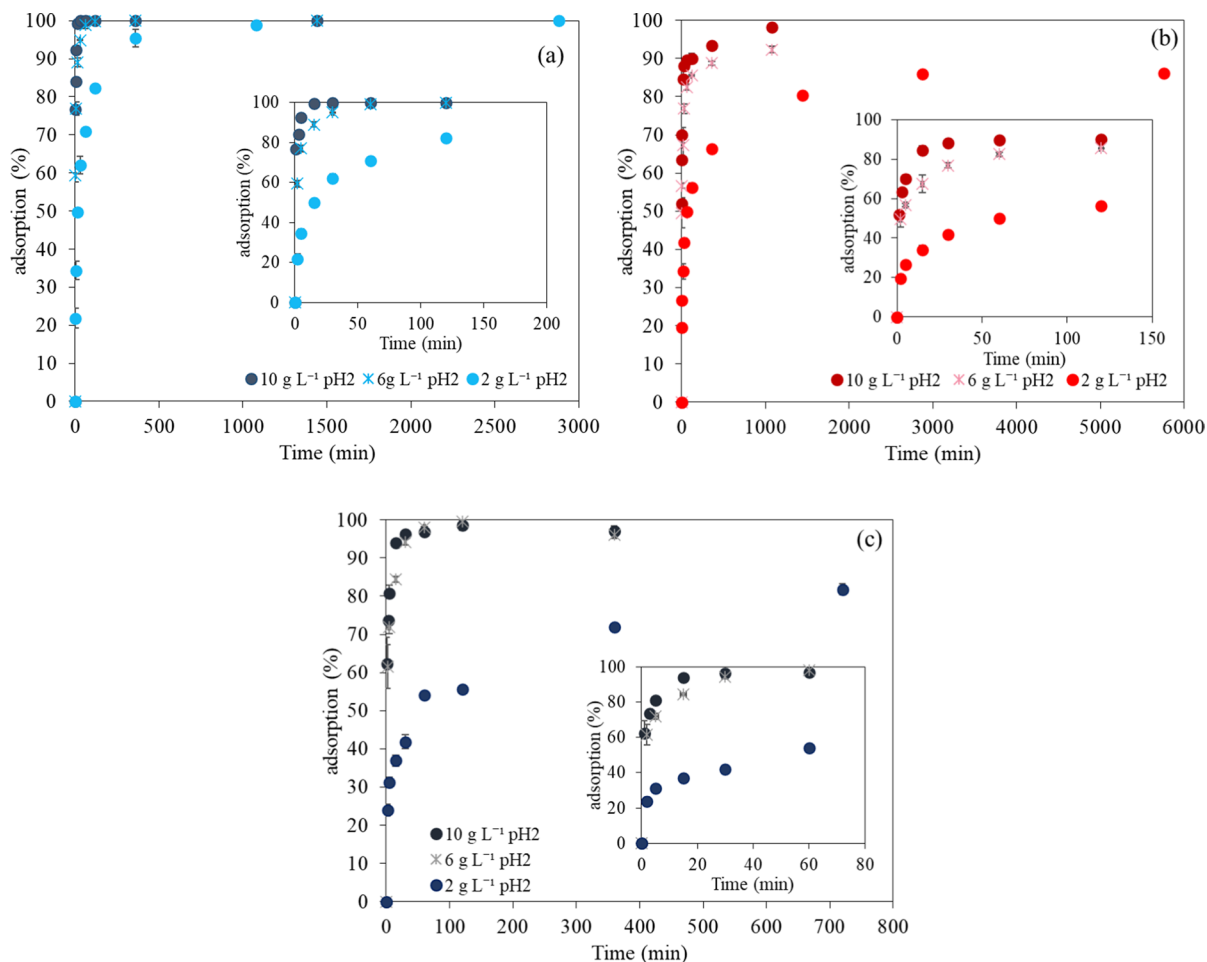


Fig. 6 Effect of adsorbent dosage on the adsorption efficiency of blue **a**, red **b** and black **c** dyes using PS (initial dye concentration 5 mg L⁻¹; pH 2; adsorbent dose 2, 6 and 10 g L⁻¹; temperature 25 °C and agitation speed 210 rpm)

driving force (Esmaili and Foroutan 2019; Khataee et al. 2013). Then, to investigate the efficiency of PS at the optimal pH to remove high dye concentrations, initial dye concentration was increased from 5 to 300 mg L⁻¹. Due to this increase, firstly the highest adsorbent dose (10 g L⁻¹) was used to determine if total dyes removal was achieved. The results obtained are shown in Fig. 7.

It is observed that at 300 mg L⁻¹ the dye removal percentage decreased with respect to that obtained for 5 mg L⁻¹ which demonstrates the influence of initial concentration. The adsorption efficiency of PS decreased from 100.0, 98.3 and 98.6% to 85.6, 63.8 and 57.0% for the blue, red and black dyes, respectively, at equilibrium (48 h), for blue and red and for a contact time of 12 h for the black dye due to the

aforementioned stability problems. This reduction could be explained since the increase of initial dye concentration causes a saturation in the total number of active binding sites which increases the repulsion by the electrostatic force between the adsorbed and non-adsorbed dye molecules (Bortoluz et al. 2020; Esmaili and Foroutan 2019). Moreover, perhaps the surface area generated by ultra-micropores could not be available for the dyes due to size-exclusion. Although increasing the initial dye concentration from 5 to 300 mg L⁻¹ reduced the removal efficiency, an increase of the maximum adsorption capacity occurred from 0.50 to 27.47 mg g⁻¹ for the blue dye, from 0.48 to 18.55 mg g⁻¹ for the red dye and from 0.40 to 16.62 mg g⁻¹ for the black one. The increase in the initial dye concentration caused

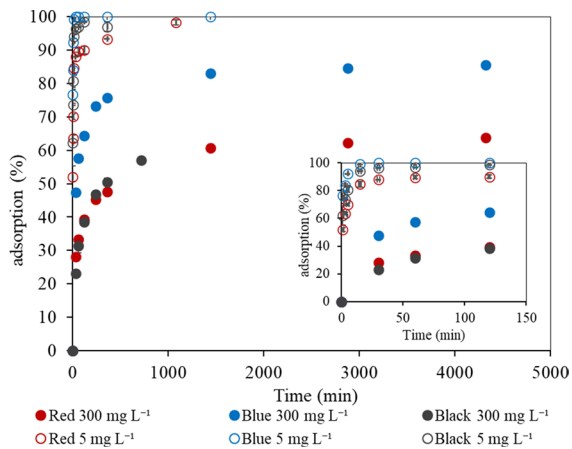


Fig. 7 Effect of initial dye concentration on dyes removal (initial dye concentration 5 and 300 mg L⁻¹; adsorbent dose 10 g L⁻¹; pH 2; temperature 25 °C; agitation speed 210 rpm)

a strong interaction between the adsorbent and the dye molecules that resulted from the increase in the driving force of the concentration gradient (Şentürk and Yildiz 2020). Thus, for 300 mg L⁻¹ the maximum

adsorption capacity increased and for the blue dye, the adsorption capacity was very close to the theoretical maximum value (30 mg g⁻¹). This could be due to differences in the dyes functional groups that lead to different interactions between the sorbent and the sorbate.

Finally, Fig. 8 shows the SEM analysis results for PS after dye adsorption at a 5000× magnification. It can be observed that after the adsorption process the PS surface is covered by the dyes. Moreover, the presence of new elements that belong to the dyes could be confirmed by EDX analysis (Table 4).

Adsorption kinetics

Kinetic behavior and the controlling mechanisms involved in the adsorption process as diffusion control, mass transfer or chemical reaction could be predicted using some kinetic models (Şentürk and Yildiz 2020). Therefore, to explain the kinetics of dye removal using un-treated pine sawdust, the experimental data was fitted to the pseudo-first order (Eq. 4), pseudo-second order (Eq. 5), and intraparticle

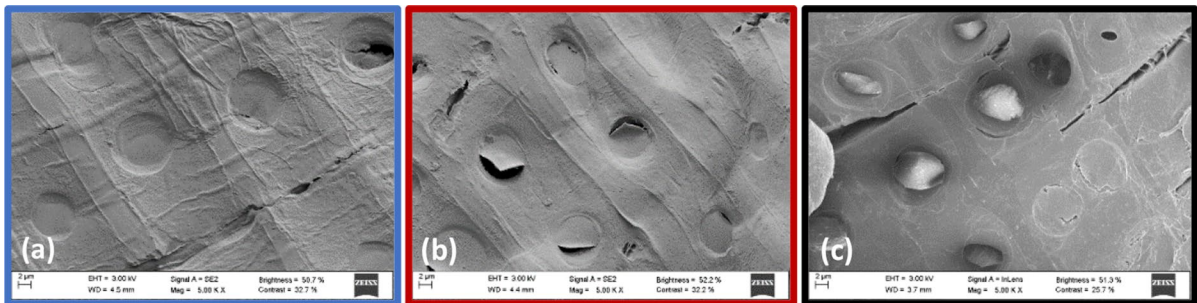


Fig. 8 SEM images of pine sawdust after adsorption of blue **a**, red **b** and black **c** wood dyes (initial dye concentration 300 mg L⁻¹; pH 2; adsorbent dose 10 g L⁻¹; temperature

25 °C; equilibrium time for blue and red dyes and maximum adsorption time for the black one; agitation speed 210 rpm)

Table 4 EDX of PS before and after dye adsorption (pH 2; initial dye concentration 300 mg L⁻¹ for blue and red and 5 mg L⁻¹ for black; equilibrium time)

Material	wt%											
	C	O	Al	Cu	K	Ca	Mg	S	N	Cl	Cr	
PS	58.6±0.1	38.8±0.1	2.0±0.1	0.3±0.0	0.1±0.0	0.1±0.0	0.1±0.0	–	–	–	–	
PS + Blue	57.6±0.1	42.3±0.1	–	–	–	–	–	0.1±0.0	–	–	–	
PS + Red	58.0±0.3	34.9±0.3	0.1±0.1	1.3±0.1	–	–	–	0.2±0.0	5.0±0.4	0.5±0.0	–	
PS + Black	66.6±1.0	28.0±1.0	–	–	–	–	–	1.5±0.2	–	1.4±0.2	2.5±0.4	

diffusion (Eq. 6) kinetic models. The kinetic parameters obtained are listed in Table 5. Kinetic constants and correlation coefficients were obtained by plotting $\log(q_e - q_t)$ versus t for the pseudo-first order model, t/q_t against t for the pseudo-second order model and q_t versus $t^{1/2}$ for the intraparticle diffusion model.

In view of the results, the predicted adsorption capacities ($q_{e, \text{calc}}$) for the pseudo-first order model were found to be much lower than the experimental ones ($q_{e, \text{exp}}$) as consequence of the low correlation coefficients obtained in most cases. This demonstrates that this model is not suitable to describe the adsorption process. However, the second order model is the one that best fits the experimental data with correlation coefficients higher than 0.975 and lower sum of square error (SSR) values for all dyes and conditions essayed and a good agreement between the experimental q_e and that predicted by the model ($q_{e, \text{calc}}$) was obtained. Regarding the intraparticle diffusion kinetic model, the kinetics of the adsorption process was divided into two linear regions (1) lower contact times and rapid uptake and (2) higher contact times and slow uptake until reaching equilibrium. In most of the experiments, high correlation coefficients (> 0.9) were obtained for the first region corroborated by a low SSR, which suggests the possibility of intraparticle diffusion of the dye from the outer surface into the pores of the sawdust at the initial phase of the adsorption process. However, the low correlation coefficients for the second region indicate a change in the adsorption mechanism.

In summary, the pseudo-second order kinetic model can describe the whole adsorption process through a chemical sorption mechanism involving valence forces due to the interchange of electrons. Simultaneously, the intraparticle diffusion kinetic model also explains the adsorption process at the initial stage with the transfer of the dye from the outer surface into the pores of the material (Şentürk and Yildiz 2020; Semerjian 2018).

Adsorption equilibrium

To better understand the mechanism of adsorption, the equilibrium data for the blue, red and black dyes on PS were obtained and fitted to the Langmuir, Freundlich, Temkin and Dubinin-Radushkevich models (Fig. 9). The study was performed considering the optimal adsorbent dose selected for low

concentrations (6 g L^{-1}) and from the results obtained it was possible to establish the limit initial dye concentration to achieve dyes removal equal to or greater than 90% (50 mg L^{-1} , 25 mg L^{-1} and 12.5 mg L^{-1} for blue, red and black dyes, respectively). Langmuir model assumes the presence of a homogeneous surface with a limited number of adsorption sites without transmigration of the adsorbate molecules onto the surface, with equal energies of adsorption, leading to monolayer adsorption. Freundlich model describes adsorption as a multilayer process with different energy levels due to the heterogeneous surface (Şentürk and Yildiz 2020; Esmaeili and Foroutan 2019). Temkin model considers that the adsorption heat of the molecules reduces in a linear way with the increase in coverage of the adsorbent surface. That adsorption is distinguished by a uniform distribution of binding energies up to a maximum. Dubinin-Radushkevich (D-R) isotherm represents a mechanism of adsorption with a Gaussian energy spreading on a heterogeneous surface. Thus, this model suggests at first a pore-filling mechanism followed by adsorption and allows to distinguish if it is going to occur a chemical or a physical adsorption through the isotherm parameters regarding sorption energy (Chandarana et al. 2020; Şentürk and Yildiz 2020).

From Fig. 9, the isotherm models that best fitted the experimental data for all cases were the Freundlich and the D-R models which do not tend to a saturation condition when adsorbate concentration in solution increases and consider that the adsorbent surface is heterogeneous (Deniz and Dogan 2022; Şentürk and Yildiz 2020). The parameters for each model are presented in Table 6.

As can be seen, both Freundlich and D-R isotherms presented the best fits with high correlation coefficients (> 0.98) and generally with the lower SSR. Freundlich isotherm with n values higher than 1 suggests a favorable adsorption and implies the presence of a heterogeneous surface with reversible adsorption and multilayer formation). The adsorbate concentration in the adsorbent increases with increasing the adsorbate concentration in solution which leads to a non-saturation behavior as shown in Fig. 9 (Bortoluz et al. 2020; Şentürk and Yildiz 2020). The adsorption equilibrium data were also satisfactorily fitted to the D-R isotherm model which considers that a pore-filling mechanism is also involved in a heterogeneous surface and is very useful for predicting the type of

Table 5 Pseudo-first, pseudo-second order and intraparticle diffusion kinetic model parameters

Dye (g L ⁻¹)	Pseudo-first order				Pseudo-second order				Intraparticle diffusion								
	q _{e,exp} (mg g ⁻¹)	k ₁ (min ⁻¹)	q _{e,calc} (mg g ⁻¹)	R ²	SSR	k ₂ (g mg ⁻¹ min ⁻¹)	q _{e,calc} (mg g ⁻¹)	R ²	SSR	k _{1,1} (mg g ⁻¹ min ^{1/2})	k _{1,2} (mg g ⁻¹ min ^{1/2})	C _i (mg g ⁻¹)	R ₁ ²	R ₂ ²	SSR ₁	SSR ₂	
<i>Natural pH, 5 mg L⁻¹</i>																	
Blue 5 g L ⁻¹	0.51 ± 0.02	9.21 × 10 ⁻⁴	0.34	0.644	0.40	4.15 × 10 ⁻²	0.46	0.995	0.037	1.69 × 10 ⁻²	2.00 × 10 ⁻⁴	0.024	0.450	0.963	0.030	4.02 × 10 ⁻³	4.14 × 10 ⁻³
Blue 10 g L ⁻¹	0.37 ± 0.03	2.07 × 10 ⁻³	0.22	0.783	0.34	1.41 × 10 ⁻¹	0.35	0.998	0.014	2.14 × 10 ⁻²	7.00 × 10 ⁻⁴	0.031	0.317	0.951	0.448	2.09 × 10 ⁻³	1.21 × 10 ⁻³
Red 5 g L ⁻¹	0.28 ± 0.02	4.61 × 10 ⁻⁴	0.22	0.920	0.47	1.53 × 10 ⁻²	0.26	0.975	0.0091	7.20 × 10 ⁻³	2.60 × 10 ⁻³	0.002	0.074	0.965	0.989	1.32 × 10 ⁻²	2.42 × 10 ⁻¹
Red 10 g L ⁻¹	0.16 ± 0.00	2.99 × 10 ⁻³	0.11	0.955	0.035	3.24 × 10 ⁻¹	0.15	0.995	0.0043	7.80 × 10 ⁻³	3.00 × 10 ⁻⁴	0.013	0.137	0.931	0.149	1.93 × 10 ⁻³	4.10 × 10 ⁻⁴
Black 5 g L ⁻¹	0.18 ± 0.00	3.22 × 10 ⁻³	0.15	0.969	0.0072	6.64 × 10 ⁻²	0.17	0.994	0.0031	6.00 × 10 ⁻³	4.00 × 10 ⁻⁴	0.006	0.144	0.970	0.289	4.03 × 10 ⁻⁴	4.48 × 10 ⁻⁴
Black 10 g L ⁻¹	0.18 ± 0.00	1.15 × 10 ⁻³	0.11	0.578	0.083	1.67 × 10 ⁻¹	0.17	0.995	0.0022	9.10 × 10 ⁻³	6.00 × 10 ⁻⁴	0.018	0.132	0.957	0.510	7.39 × 10 ⁻⁴	5.71 × 10 ⁻⁴
<i>pH 2, 5 mg L⁻¹</i>																	
Blue 10 g L ⁻¹	0.50 ± 0.00	3.12 × 10 ⁻¹	0.24	0.943	0.65	8.59	0.50	1.000	0.0029	2.02 × 10 ⁻¹	7.00 × 10 ⁻⁵	0.065	0.498	0.848	0.286	2.07 × 10 ⁻²	9.89 × 10 ⁻⁶
Blue 6 g L ⁻¹	0.70 ± 0.00	4.31 × 10 ⁻²	0.23	0.869	1.81	1.23	0.70	1.000	0.0027	1.58 × 10 ⁻¹	7.00 × 10 ⁻⁴	0.097	0.678	0.854	0.355	3.35 × 10 ⁻²	6.56 × 10 ⁻⁴
Blue 2 g L ⁻¹	1.99 ± 0.00	3.68 × 10 ⁻³	1.04	0.906	8.59	2.90 × 10 ⁻²	2.00	1.000	0.16	1.79 × 10 ⁻¹	8.30 × 10 ⁻³	0.165	1.610	0.943	0.710	7.81 × 10 ⁻²	2.94 × 10 ⁻²
Red 10 g L ⁻¹	0.48 ± 0.00	5.99 × 10 ⁻³	0.13	0.488	1.17	4.82 × 10 ⁻¹	0.48	1.000	0.050	1.54 × 10 ⁻¹	2.00 × 10 ⁻³	0.038	0.421	0.906	0.929	6.99 × 10 ⁻³	1.92 × 10 ⁻⁴
Red 6 g L ⁻¹	0.75 ± 0.01	6.91 × 10 ⁻³	0.25	0.655	2.11	2.34 × 10 ⁻¹	0.75	1.000	0.057	1.35 × 10 ⁻¹	4.00 × 10 ⁻³	0.099	0.632	0.815	0.824	3.26 × 10 ⁻²	1.65 × 10 ⁻³
Red 2 g L ⁻¹	2.06 ± 0.01	1.61 × 10 ⁻³	1.24	0.864	7.53	1.11 × 10 ⁻²	2.07	1.000	0.54	1.42 × 10 ⁻¹	1.13 × 10 ⁻²	0.191	1.341	0.916	0.833	7.42 × 10 ⁻²	7.06 × 10 ⁻²

Table 5 (continued)

Dye (g L ⁻¹)	Pseudo-first order			Pseudo-second order			Intraparticle diffusion											
	q _{e,exp} (mg g ⁻¹)	k ₁ (min ⁻¹)	q _{e,calc} (mg g ⁻¹)	R ²	SSR	k ₂ (g mg ⁻¹ min ⁻¹)	q _{e,calc} (mg g ⁻¹)	R ²	SSR	k _{1,1} (mg g ⁻¹ min ^{1/2})	k _{1,2} (mg g ⁻¹ min ^{1/2})	C _i (mg g ⁻¹)	C _{i-1} (mg g ⁻¹)	R ₁ ²	R ₂ ²	SSR ₁	SSR ₂	
Black 10 g L ⁻¹	0.40±0.00	6.22×10 ⁻²	0.12	0.752	0.63	6.95	0.40	1.000	0.0061	1.46×10 ⁻¹	7.00×10 ⁻⁴	0.039	0.388	0.889	0.322	7.52×10 ⁻³	1.29×10 ⁻⁴	
Black 6 g L ⁻¹	0.72±0.00	6.08×10 ⁻²	0.35	0.922	1.03	4.05	0.70	1.000	0.046	1.52×10 ⁻¹	3.00×10 ⁻⁴	0.108	0.698	0.823	0.011	3.89×10 ⁻²	9.25×10 ⁻⁴	
Black 2 g L ⁻¹	1.45±0.01	1.01×10 ⁻²	0.96	0.799	2.11	4.72×10 ⁻²	1.47	0.989	0.24	1.91×10 ⁻¹	4.27×10 ⁻²	0.109	0.651	0.871	0.987	4.21×10 ⁻²	2.60×10 ⁻³	
<i>pH 2, 300 mg L⁻¹</i>																		
Blue 10 g L ⁻¹	27.47±0.20	2.53×10 ⁻³	11.02	0.866	2333.17	1.11×10 ⁻³	27.93	1.000	7.14	1.97	7.79×10 ⁻²	1.867	23.181	0.924	0.890	20.29	1.42	
Red 10 g L ⁻¹	18.55±0.30	2.32×10 ⁻³	10.83	0.950	544.71	7.52×10 ⁻⁴	19.19	0.999	13.38	1.09	1.13×10 ⁻¹	0.906	12.336	0.943	0.887	4.63	3.06	
Black 10 g L ⁻¹	16.62±0.04	4.84×10 ⁻³	11.93	0.863	173.35	1.15×10 ⁻³	17.09	0.976	14.68	1.25	4.04×10 ⁻¹	0.355	6.040	0.955	0.904	2.33	2.33	

*1: first stage of ID; 2: second stage of ID; SSR: Sum of square error; R: correlation coefficient

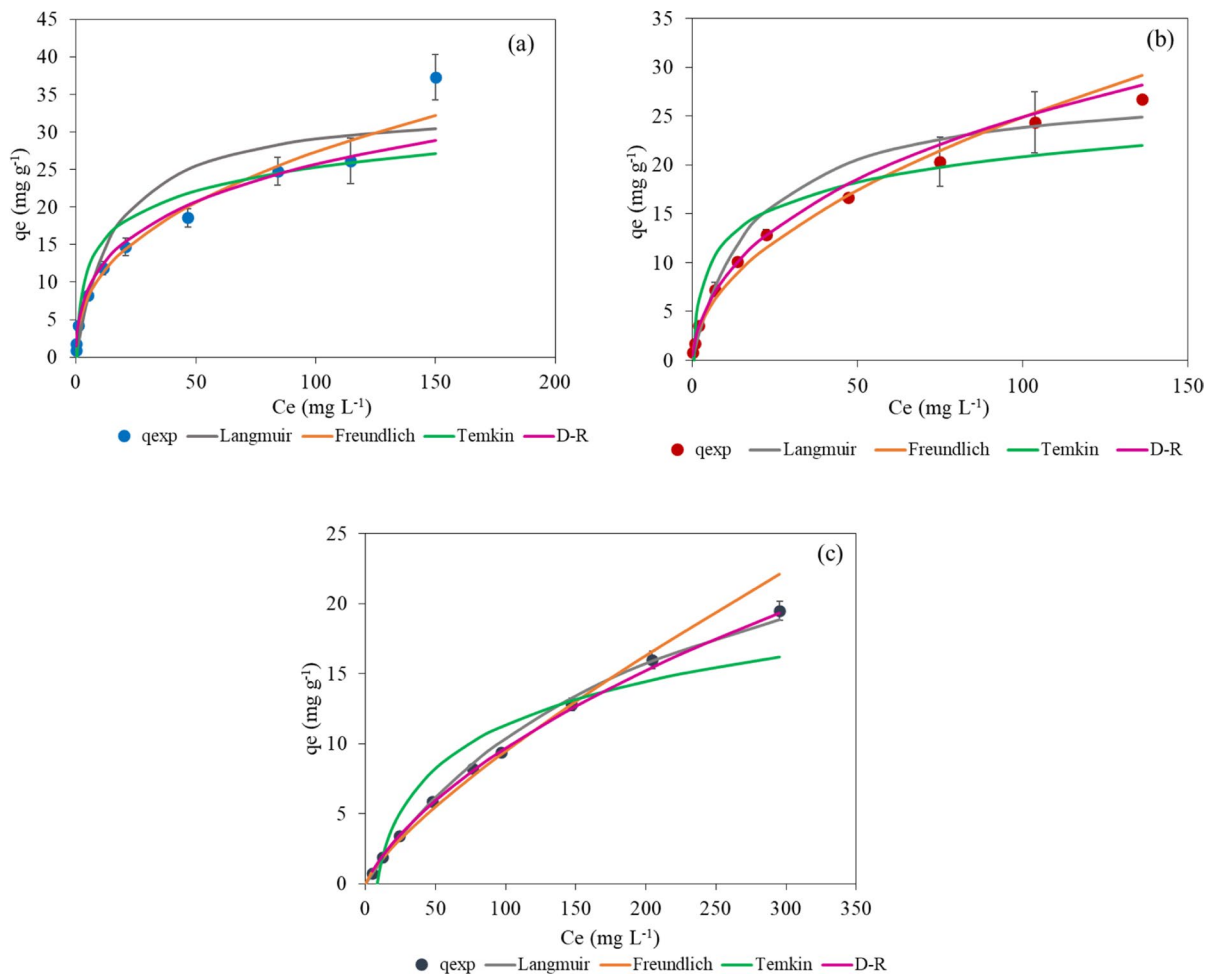


Fig. 9 Adsorption isotherms of blue **a**, red **b** and black **c** dyes by pine sawdust (initial dye concentration 5–300 mg L⁻¹; adsorbent dose 6 g L⁻¹; pH 2; time 4 days for blue and red and 12 h for black; temperature 25 °C; agitation speed 210 rpm)

adsorption through the mean adsorption energy (E) parameter. If E is lower than 8 kJ mol^{-1} a physisorption process occurs with van der Waals interactions. However, if $8 < E < 16 \text{ kJ mol}^{-1}$ adsorption is a chemical process with high adsorption enthalpy because of the ion-exchange mechanism (Deniz and Dogan 2022; Şentürk and Yıldız 2020). Moreover, the values of the monolayer saturation capacity, $q_{m,D}$, in D-R equation are significantly higher than those for the maximum adsorption capacity, q_m , in the Langmuir one since $q_{m,D}$ represents the total specific meso and macropore volume of the biosorbent. Considering this, PS could be considered a porous biosorbent in agreement with the above-mentioned characterization (Horciu et al. 2020). The adsorption mechanism is

very important to understand the basis of the adsorption process. Based on the most common functional groups present on pine sawdust (Orozco et al. 2023) and similar to those described in literature, such as carboxyl, phenolic or hydroxyl (Bortoluz et al. 2020; Salazar-Rabago et al. 2017; Şentürk and Yıldız 2020) and also on the results from the adsorption kinetic and equilibrium studies an adsorption mechanism was proposed (Fig. 10).

The maximum adsorption capacities (q_m) calculated by the Langmuir model (33.78 mg g^{-1} for blue and 28.41 mg g^{-1} for red) are close to the experimental q_{max} obtained (37.30 mg g^{-1} for blue and 26.78 mg g^{-1} for red), except for black dye (q_m calculated: 32.47 mg g^{-1} and q_{max} obtained: 19.47 mg g^{-1})

Table 6 Parameters of isotherm models for the adsorption of the blue, red and black dyes on pine sawdust

Isotherms	Parameters	Blue dye	Red dye	Black dye
Langmuir	q_m (mg g^{-1})	33.78	28.41	32.47
	K_L (L mg^{-1})	0.062	0.052	0.0047
	R_L ($5\text{--}300 \text{ mg L}^{-1}$)	0.764–0.051	0.796–0.060	0.977–0.415
	R^2	0.912	0.963	0.980
	SSR	142.93	30.79	32.04
Freundlich	n	2.47	1.95	1.28
	K_F ($\text{mg g}^{-1} (\text{L mg}^{-1})^{-1/n}$)	4.22	2.34	0.26
	R^2	0.994	0.991	0.993
	SSR	37.36	12.43	53.02
Temkin	B (J mol^{-1})	4.52	3.77	4.48
	K_T (L mg^{-1})	2.67	2.51	0.13
	R^2	0.829	0.868	0.904
	SSR	287.63	104.39	35.65
Dubidin-Radushkevich	$q_{m,D}$ (mg g^{-1})	91.47	137.61	217.41
	K_{DR} ($\text{mol}^2 \text{kJ}^{-2}$)	2.82×10^{-9}	3.97×10^{-9}	6.05×10^{-9}
	E (kJ mol^{-1})	13.32	11.22	9.09
	R^2	0.984	0.996	0.997
	SSR	139.70	8.14	0.51

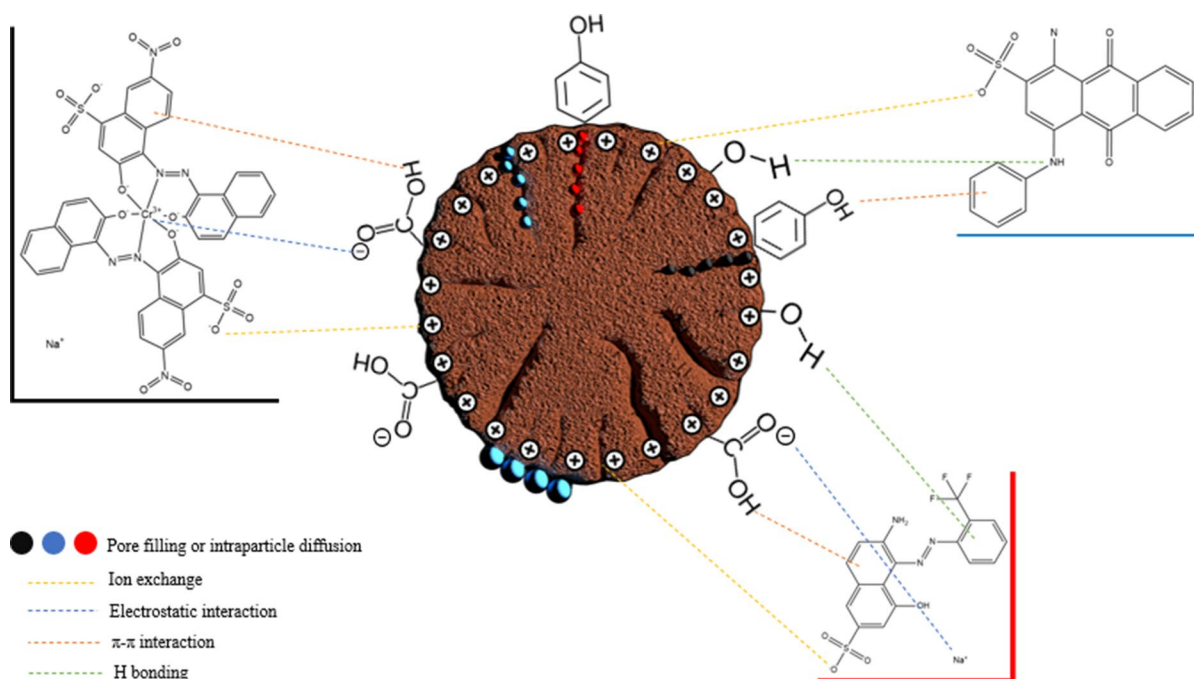


Fig. 10 Proposed mechanism for blue, red and black dye adsorption by un-treated PS

which could be due to and insufficient contact time for high concentrations. R_L values obtained for the three dyes between 0 and 1 indicate favorable adsorption,

although it is more favorable at low concentrations since R_L is closer to 1 (Al-Khadi 2020; Şentürk and Yildiz 2020). Regarding the Temkin isotherm, which

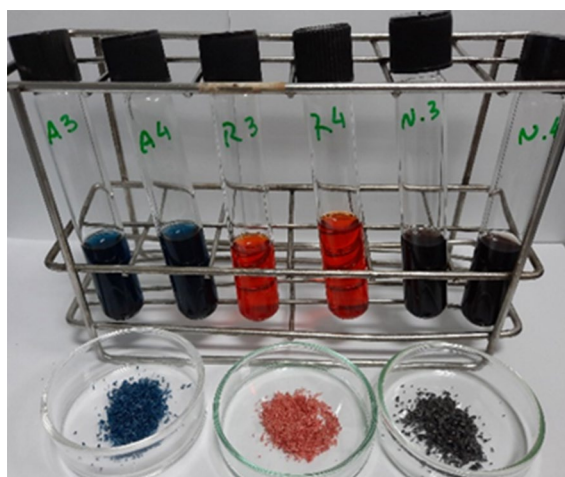
Table 7 Application of various bioadsorbents for dyes removal

Material	Treatment	Dye	Conditions*	q_m (mg g ⁻¹)	References
<i>Pinus radiata</i> sawdust	–	Blue for wood	Dose: 2–10 g L ⁻¹ ; C: 5–300 mg L ⁻¹ ; pH: 2–9; T: 25 °C	27.5	In this study
<i>Pinus radiata</i> sawdust	–	Red for wood	Dose: 2–10 g L ⁻¹ ; C: 5–300 mg L ⁻¹ ; pH 2–9; T: 25 °C	18.6	In this study
<i>Pinus radiata</i> sawdust	–	Black for wood	Dose: 2–10 g L ⁻¹ ; C: 5–300 mg L ⁻¹ ; pH 2–9; T: 25 °C	16.6	In this study
<i>Pinus pinaster</i> bark	Washed	Congo red	pH: 2–9; dose: 1–10 g L ⁻¹ ; T: 25–60 °C; C: 5 mg L ⁻¹	0.3–1.6	Litefti et al. (2019)
Pinecone	Washed	Methylene blue	Dose: 2 g L ⁻¹ ; C: 50–250 mg L ⁻¹ ; T: 25–50 °C	125	Özdemir (2019)
Pine sawdust	Pre-treated	Maxilon Red GRL	pH: 6; T: 25 °C; C: 250 mg L ⁻¹ ; dose: 8 g L ⁻¹	312.5	Şentürk and Yildiz (2020)
<i>Casuarina equisetifolia</i> pines	Washed	Methylene blue	Dose: 0.5 g L ⁻¹ ; C: 100 mg L ⁻¹ ; pH: 7	41.4	Chandarana et al. (2021)
Aleppo Pine cones	Washed	Methylene blue	C: 100 mg L ⁻¹ ; dose: 0.5 g L ⁻¹ ; pH 10	93.6	Elmoubarki et al. (2016)
White Pine (<i>Pinus durangensis</i>) sawdust	Washed	Methylene blue	T: 15–35 °C; pH: 3–10; C: 300 mg L ⁻¹ ; dose: 2 g L ⁻¹	70.0	Salazar-Rabago et al. (2017)
Cedar sawdust	–	Methylene blue	pH: 2–12; C: 50–2000 mg L ⁻¹ ; T: 25–60 °C; dose: 5 g L ⁻¹	100	Fayoud et al. (2015)
Pine sawdust	–	Methylene blue	pH: 2–12; C: 50–2000 mg L ⁻¹ ; T: 25–60 °C; dose: 10 g L ⁻¹	71.4	Fayoud et al. (2015)
Wheat straw	–	Methylene blue	pH: 2–12; C: 50–2000 mg L ⁻¹ ; T: 25–60 °C; dose: 5 g L ⁻¹	143	Fayoud et al. (2015)
Provence cane <i>Arundo donax</i>	–	Methylene blue	pH: 2–12; C: 50–2000 mg L ⁻¹ ; T: 25–60 °C; dose: 5 g L ⁻¹	91	Fayoud et al. (2015)
Turkish red pine sawdust	Pre-treated	Acid blue 256	pH: 2; C: 200 mg L ⁻¹ ; dose 1 g L ⁻¹ ; T: 25 °C	54.2	Can (2015)
Pine Cone	Washed	Acid black 26	C: 50 mg L ⁻¹ ; pH: 2; dose: 1 g L ⁻¹ ; T: 25–65 °C;	57.5	Mahmoodi et al. (2011)
Pine Cone	Washed	Acid blue 7	C: 50 mg L ⁻¹ ; pH: 2; dose: 2 g L ⁻¹ ; T: 25–65 °C;	31.6	Mahmoodi et al. (2011)
Oak leaves	Washed	Methylene blue	C: 50 mg L ⁻¹ ; dose: 0.1 g L ⁻¹ ; pH: 7; T: 25 °C	33.5	Sulyman and Gierak (2020)
Pine tree cones (<i>P. radiata</i>)	Washed	Congo Red	pH: 3.55; C: 20 mg L ⁻¹ ; T: 30 °C; dose: 0.4 g L ⁻¹	32.7	Dawood and Sen (2012)
Pine tree cones (<i>P. radiata</i>)	Pre-treated	Congo Red	pH: 3.55; C: 20 mg L ⁻¹ ; T: 30 °C; dose: 0.4 g L ⁻¹	40.2	Dawood and Sen (2012)

*Dose: adsorbent dose; C: Initial dye concentration; T: Temperature

Table 8 Desorption percentage of dyes from dye loaded PS using NaOH 0.1 M and HCl 0.1 M

Dye	%Desorption (HCl)	%Desorption (NaOH)
Blue	0.38 ± 0.03	16.26 ± 0.56
Red	0.70 ± 0.01	90.86 ± 0.52
Black	0.91 ± 0.02	24.75 ± 0.02

**Fig. 11** Dye color intensity in replicated samples after the last desorption stage from dye loaded PS using NaOH 0.1 M and PS material after desorption (Adsorption stage: pH=2, dye concentration 300 mg L⁻¹; adsorbent dose 10 g L⁻¹; contact time 4 days for blue and red and 12 h for black; temperature 25 °C; agitation speed 210 rpm; desorption stage: adsorbent dose 50 g L⁻¹; contact time 4 h; temperature 25 °C; agitation speed 350 rpm)

implies adsorbent interactions between the adsorbent and the adsorbate, model fitting was worse than with the other models. The positive values of B_T suggest that the adsorption reaction is endothermic (Collins et al. 2019). Fig. 9 shows that the experimental data do not tend to saturation as the Langmuir or Temkin models predict and correlation coefficients were lower than for Freundlich and D-R models.

Bortoluz et al. (2020) and Esmaeili and Foroutan (2019) showed that the Freundlich model was also the one that better described the adsorption of methylene blue by *Pinus elliotti* sawdust and by sawdust of palm trees, eucalyptus and sour lemon, respectively. Moreover, Blaga et al. (2022) and Deniz and Dogan (2022) also reported a great fit to the D-R isotherm

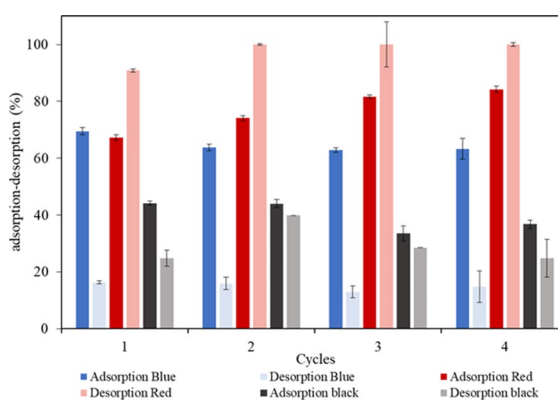
model for dye adsorption by biosorbents based on waste biomass.

Table 7 summarizes the adsorption capacity of different bioadsorbents, mostly from pine species, for the adsorption of blue, red and black dyes under different experimental conditions.

Desorption and regeneration of the adsorbent

The adsorption process can be considered more operative and economical if the material used can be regenerated and reused in several adsorption/desorption cycles (El Messaoudi et al. 2021; Kamran et al. 2022). Furthermore, dye loaded material can cause a waste disposal problem, so the study of the desorption process acquires a significant role (Mirza and Ahmad 2020). Ion exchange mechanisms can be involved on dye desorption using relatively economical acids, salts, organic acids and bases (Mashkoor et al. 2018). In this work the maximum dye adsorption capacity was achieved at acid pH, so to validate if desorption efficiency is improved in basic medium desorption experiments were carried out comparing HCl 0.1 M and NaOH 0.1 M as desorption agents and the results are shown in Table 8.

Sodium hydroxide led to significantly higher desorption efficiencies than hydrochloric acid for all dyes, mainly for the red one with a high desorption percentage above 90%, although the solid

**Fig. 12** Adsorption and desorption cycles of blue, red and black dyes onto PS (Adsorption stage: pH=2, dye concentration 300 mg L⁻¹; adsorbent dose 10 g L⁻¹; contact time 4 days for blue and red and 12 h for black; temperature 25 °C; agitation speed 210 rpm; desorption stage: adsorbent dose 50 g L⁻¹; contact time 4 h; temperature 25 °C; agitation speed 350 rpm)

material preserves some color. As well, as illustrated by Fig. 11, although the adsorption percentages for the blue and black dyes are not greater than 25%, it is possible to observe the high color intensity in these experiments proving the effectiveness of NaOH as desorption agent. This behavior can be explained considering that at basic pH the number of negative charges on the adsorbent surface significantly increases and leads to electrostatic repulsion between the dye components and the adsorbent and, therefore, the dye desorbs from the adsorbent surface. Additionally, alkali components break the connection between the adsorbate and the adsorbent through a chemical reaction (Hu et al. 2020). By the contrary, the lower dye desorption from PS for blue and black dyes indicates a stronger interaction between the adsorbent and the adsorbate, usually by chemisorption which is irreversible contrary to electrostatic interactions (Salazar-Rabago et al. 2017). High desorption efficiencies in alkaline medium as for red dye were also obtained by Kamran et al. (2022) and El Messaoudi et al. (2021) for the desorption of acid red 1 from chemically modified sugarcane bagasse and congo red from date stones and jujube shells, respectively.

The reusability of PS for dye adsorption was investigated by repeating the adsorption–desorption process up to four times using a 0.1 M NaOH solution for desorption. The results are presented in Fig. 12.

High desorption percentages between 91 and 100% were achieved for the red dye and the adsorption percentage increased from 67 to 84% in subsequent cycles. An improvement occurs from the first to the fourth adsorption stage with a decrease on the red color intensity. This could be explained considering that NaOH is one of the most common chemical activating agents used to enhance the adsorbent surface and increase its adsorption efficiency (Şentürk and Yildiz 2020; Azzaz et al. 2016). Desorption efficiency of red dye can be increased by electrostatic repulsion between negatively charged sites on the PS and anionic dye molecules. In addition, the abundance of OH⁻ ions in the basic solution and its exchange with dye ions on PS could increase the desorption efficiency depending on the dye structure (Daneshvar et al. 2017). These results confirm that, in the case of the red dye, PS offers the potential to be used at least four times with an increase of about 17% in the removal efficiency.

The regeneration input revealed that a slight decrease, about 7–11% in the adsorption percentage, occurs as the PS is reused for blue and black dyes which can be explained by the progressive accumulation of dye molecules on the PS surface owed to the lower desorption percentages that promotes adsorbent exhaustion. Nevertheless, PS can be reused at least four times without significant loss on the adsorption percentage. Similar results, with the slight decrease in the adsorption percentage at each cycle for congo red and crystal violet dyes were observed by El Messaoudi et al. (2021) and Mashkoor et al. (2018) respectively.

Conclusions

Pine sawdust was used as an adsorbent for the removal of wood dyes for wastewater treatment. The effect of some parameters on the adsorption efficiency was studied and the results obtained showed that the highest removal efficiency occurred at pH 2 and increased with increasing contact time till equilibrium was reached and adsorbent dose, except for blue wood dye that reached 100% in all cases. Based on contact time and removal percentage the optimum adsorbent dose for dyes removal was 6 g L⁻¹. On the other hand, removal efficiency decreased with increasing initial dye concentration.

The kinetics of dye adsorption was better explained by the pseudo-second order kinetic model characteristic of a chemical adsorption mechanism. Also, the first stage of the adsorption process could be described by the intraparticle diffusion model with dye transfer into the pores of the material.

The adsorption equilibrium study revealed that the models that better represented the adsorption process for the blue, red and black dyes was the Freundlich and D-R isotherms that describes a heterogeneous surface and a multilayer process.

Sodium hydroxide, showing desorption efficiencies of 16.3%, 90.9% and 24.8% for the blue, red and black dyes, respectively, in the first adsorption/desorption cycle, was selected as desorption agent. It was demonstrated that the sorbent can be reused at least in four consecutive adsorption/desorption cycles for the red dye desorption with improved removal efficiencies.

Regarding the blue and black dyes, the desorption efficiency achieved lower values but did not lead to a significant decrease in the adsorption percentage and could be applied if considering combining adsorption–desorption with an additional post-treatment stage to improve the regeneration of adsorbent or including, so as not to add another stage, testing the desorbing agents under different conditions.

The obtained results showed that pine sawdust is an efficient adsorbent to remove wood dyes from aqueous solutions and factors such as pH, contact time and initial dye concentration influence dye sorption and removal efficiency. Due to the great potential of the studied adsorbent, further studies should be performed with real textile wastewater to better understand the effect of coexisting contaminants.

Author contribution CHP: Investigation, Validation, Visualization, Writing—original draft (catypimentelster@gmail.com). MSF: Conceptualization, Methodology, Supervision, Funding acquisition, Writing—review & editing (maria Sonia.freire@usc.es). DG-D: Conceptualization, Methodology, Supervision, Funding acquisition, Writing—review & editing (diego.gomez@usc.es). JG-Á: Conceptualization, Methodology, Supervision, Funding acquisition, Writing—review & editing (julia.gonzalez@usc.es).

Funding Open Access funding provided thanks to the CRUE-CSIC agreement with Springer Nature. This work was financial supported by Xunta de Galicia (ED431B 2020/039).

Data availability All data generated or analyzed during this study are included in this article.

Declarations

Conflict of interest The authors declare no competing interests.

Open Access This article is licensed under a Creative Commons Attribution 4.0 International License, which permits use, sharing, adaptation, distribution and reproduction in any medium or format, as long as you give appropriate credit to the original author(s) and the source, provide a link to the Creative Commons licence, and indicate if changes were made. The images or other third party material in this article are included in the article's Creative Commons licence, unless indicated otherwise in a credit line to the material. If material is not included in the article's Creative Commons licence and your intended use is not permitted by statutory regulation or exceeds the permitted use, you will need to obtain permission directly from the copyright holder. To view a copy of this licence, visit <http://creativecommons.org/licenses/by/4.0/>.

References

- Akhouairi S, Ouachtak H, Addi AA, Jada A, Douch J (2019) Natural sawdust as adsorbent for the eriochrome black T dye removal from aqueous solution. *Water Air Soil Poll* 230(8):1–15. <https://doi.org/10.1007/s11270-019-4234-6>
- Al-Kadhi NS (2020) Removal of fluorescein dye from aqueous solutions using natural and chemically treated pine sawdust. *Int J Anal Chem* 2020:1–9. <https://doi.org/10.1155/2020/8824368>
- Aragaw TA, Bogale FM (2021) Biomass-based adsorbents for removal of dyes from wastewater: a review. *Front Environ Sci* 9:558. <https://doi.org/10.3389/fenvs.2021.764958>
- Azzaz AA, Jellali S, Assadi AA, Bousselmi L (2016) Chemical treatment of orange tree sawdust for a cationic dye enhancement removal from aqueous solutions: kinetic, equilibrium and thermodynamic studies. *Desalination Water Treat* 57(46):22107–22119. <https://doi.org/10.1080/19443994.2015.1103313>
- Blaga AC, Tanasă AM, Cimpoesu R, Tataru-Farmus RE, Suteu D (2022) Biosorbents based on biopolymers from natural sources and food waste to retain the methylene blue dye from the aqueous medium. *Polymers* 14(13):1–14. <https://doi.org/10.3390/polym14132728>
- Bortoluz J, Ferrarini F, Bonetto LR, da Silva CJ, Giovanela M (2020) Use of low-cost natural waste from the furniture industry for the removal of methylene blue by adsorption: isotherms, kinetics and thermodynamics. *Cellulose* 27(11):6445–6466. <https://doi.org/10.1007/s10570-020-03254-y>
- Can M (2015) Equilibrium, kinetics and process design of acid yellow 132 adsorption onto red pine sawdust. *Water Sci Technol* 71(12):1901–1911. <https://doi.org/10.2166/wst.2015.164>
- Chandarana H, Suganya S, Madhava AK (2020) Surface functionalized Casuarina equisetifolia pine powder for the removal of hetero-polyaromatic dye: characteristics and adsorption. *Int J Environ Anal Chem* 102(17):5457–5471. <https://doi.org/10.1080/03067319.2020.1798418>
- Chandarana H, Senthil Kumar P, Seenivasan M, Anil Kumar M (2021) Kinetics, equilibrium and thermodynamic investigations of methylene blue dye removal using Casuarina equisetifolia pines. *Chemosphere* 285:131480. <https://doi.org/10.1016/j.chemosphere.2021.131480>
- Chikri R, Elhadiri N, Benchanaa M, El maguana Y (2020) Efficiency of sawdust as low-cost adsorbent for dyes removal. *J Chem* 2020:17. <https://doi.org/10.1155/2020/8813420>
- Chowdhury ZZ, Ziaul Karim M, Ashraf MA, Khalid K (2016) Influence of carbonization temperature on physicochemical properties of biochar derived from slow pyrolysis of durian wood (*Durio zibethinus*) sawdust. *Bioresources* 11(2):3356–3372. <https://doi.org/10.15376/biores.11.2.3356-3372>
- Collins ON, Elijah OC, Okechukwu OD (2019) Adsorption of a dye (Crystal Violet) on an acid modified non-conventional adsorbent. *J Chem Technol Metall* 54(1):95–110
- Daneshvar E, Vazirzadeh A, Niazi A, Kousha M, Naushad M, Bhatnagar A (2017) Desorption of Methylene blue dye from brown macroalga: effects of operating parameters, isotherm study and kinetic modeling. *J Clean Prod*

- 152:443–453. <https://doi.org/10.1016/J.JCLEPRO.2017.03.119>
- Dawood S, Sen TK (2012) Removal of anionic dye Congo red from aqueous solution by raw pine and acid-treated pine cone powder as adsorbent: equilibrium, thermodynamic, kinetics, mechanism and process design. *Water Res* 46(6):1933–1946. <https://doi.org/10.1016/j.watres.2012.01.009>
- De Meyer T, Hemelsoet K, Van Speybroeck V, De Clerck K (2014) Substituent effects on absorption spectra of pH indicators: an experimental and computational study of sulfonphthaleine dyes. *Dyes Pigm* 102:241–250. <https://doi.org/10.1016/j.dyepig.2013.10.048>
- Deniz F, Dogan F (2022) Effective cleaning of a hazardous synthetic triarylmethane-type dye from aquatic environment with a multifunctional waste biomass-based biosorbent. *Biomass Convers Biorefinery*. <https://doi.org/10.1007/s13399-021-01995-9>
- Elmoubarki R, Moufti A, Tounsadi H, Mahjoubi FZ, Farnane M, Machrouhi A, Elhalil A, Abdennouri M, Zouhri A, Barka N (2016) Kinetics and thermodynamics study of methylene blue adsorption onto Aleppo pine cones. *J Mater Environ Sci* 7(8):2869–2879
- Elwakeel KZ (2010) Environmental application of chitosan resins for the treatment of water and wastewater: a review. *J Dispersion Sci Technol* 31(3):273–288. <https://doi.org/10.1080/01932690903167178>
- Elwakeel KZ, El-Bindary AA, Ismail A, Morshidy AM (2017) Magnetic chitosan grafted with polymerized thiourea for remazol brilliant blue R recovery: effects of uptake conditions. *J Dispersion Sci Technol* 38(7):943–952. <https://doi.org/10.1080/01932691.2016.1216436>
- Esmaeili H, Foroutan R (2019) Adsorptive behavior of methylene blue onto sawdust of sour lemon, date palm, and eucalyptus as agricultural wastes. *J Dispers Sci Technol* 40(7):990–999. <https://doi.org/10.1080/01932691.2018.1489828>
- Fayoud N, Tahiri S, Alami Younssi S, Albizane A, Gallart-Mateu D, Cervera ML, de la Guardia M (2015) Kinetic, isotherm and thermodynamic studies of the adsorption of methylene blue dye onto agro-based cellulosic materials. *New Pub: Balaban* 57(35):16611–16625. <https://doi.org/10.1080/19443994.2015.1079249>
- Freundlich H (1907) Über die adsorption in lösungen. *Z Phy Chem* 57(1):385–470
- Gemici BT, Ozel HU, Ozel HB (2021) Removal of methylene blue onto forest wastes: adsorption isotherms, kinetics and thermodynamic analysis. *Environ Technol Innov* 22:101501. <https://doi.org/10.1016/j.eti.2021.101501>
- Ho YS, McKay G (1999) Pseudo-second order model for sorption processes. *Process Biochem* 34(5):451–465
- Horciu IL, Blaga AC, Rusu L, Zaharia C, Suteu D (2020) Biosorption of reactive dyes from aqueous media using the *Bacillus* sp. Residual biomass. *Desalin Water Treat* 195:353–360. <https://doi.org/10.5004/dwt.2020.25901>
- Hu L, Guang C, Liu Y, Su Z, Gong S, Yao Y, Wang Y (2020) Adsorption behavior of dyes from an aqueous solution onto composite magnetic lignin adsorbent. *Chemosphere* 246:125757. <https://doi.org/10.1016/J.CHEMOSPHERE.2019.125757>
- Ighalo JO, Zhou Y, Zhou Y, Igwegbe CA, Anastopoulos I, Raji MA, Iwuozor KO (2022) A review of pine-based adsorbents for the adsorption of dyes. *Biomass Deriv Mater Environ Appl*. <https://doi.org/10.1016/B978-0-323-91914-2.00013-1>
- Islam MT, Saenz-Arana R, Hernandez C, Guinto T, Ahsan MA, Kim H, Lin Y, Alvarado-Tenorio B, Noveron JC (2018) Adsorption of methylene blue and tetracycline onto biomass-based material prepared by sulfuric acid reflux. *RSC Adv* 8(57):32545–32557. <https://doi.org/10.1039/C8RA05395B>
- Jaouadi M (2021) Characterization of activated carbon, wood sawdust and their application for boron adsorption from water. *Int Wood Prod J* 12(1):22–33. <https://doi.org/10.1080/20426445.2020.1785605>
- Kah M, Sigmund G, Xiao F, Hofmann T (2017) Sorption of ionizable and ionic organic compounds to biochar, activated carbon and other carbonaceous materials. *Water Res* 124:673–692. <https://doi.org/10.1016/j.watres.2017.07.070>
- Kamran U, Bhatti HN, Noreen S, Tahir MA, Park SJ (2022) Chemically modified sugarcane bagasse-based biocomposites for efficient removal of acid red 1 dye: kinetics, isotherms, thermodynamics, and desorption studies. *Chemosphere* 291(P2):132796. <https://doi.org/10.1016/j.chemosphere.2021.132796>
- Kantar C, Akal H, Kaya B, Islamoğlu F, Türk M, Şaşmaz S (2015) Novel phthalocyanines containing resorcinol azo dyes; Synthesis, determination of pKa values, antioxidant, antibacterial and anticancer activity. *J Organomet Chem* 783:28–39. <https://doi.org/10.1016/j.jorganchem.2014.12.042>
- Khataee AR, Vafaei F, Jannatkah M (2013) Biosorption of three textile dyes from contaminated water by filamentous green algal *Spirogyra* sp.: kinetic, isotherm and thermodynamic studies. *Int Biodeterior Biodegrad* 83:33–40. <https://doi.org/10.1016/J.IBIOD.2013.04.004>
- Kim KC, Yoon TU, Bae YS (2016) Applicability of using CO₂ adsorption isotherms to determine BET surface areas of microporous materials. *Microporous Mesoporous Mater* 224:294–301. <https://doi.org/10.1016/j.micromeso.2016.01.003>
- Konicki W, Cendrowski K, Chen X, Mijowska E (2013) Application of hollow mesoporous carbon nanospheres as an high effective adsorbent for the fast removal of acid dyes from aqueous solutions. *Chem Eng J* 228:824–833. <https://doi.org/10.1016/j.cej.2013.05.067>
- Kumar NS, Asif M, Al-Hazzaa MI (2018) Adsorptive removal of phenolic compounds from aqueous solutions using pine cone biomass: kinetics and equilibrium studies. *Environ Sci Pollut Res* 25:21949–21960. <https://doi.org/10.1007/s11356-018-2315-5>
- Langmuir I (1918) The adsorption of gases on plane surfaces of glass, mica and platinum. *J Am Chem Soc* 40(9):1361–1403
- Litefti K, Freire MS, Stitou M, González-Álvarez J (2019) Adsorption of an anionic dye (congo red) from aqueous solutions by pine bark. *Sci Rep* 9(1):1–11. <https://doi.org/10.1038/s41598-019-53046-z>
- Lorenz M, Paganini C, Storti G, Morbidelli M (2019) Macroporous polymer-protein hybrid materials for

- antibody purification by combination of reactive gelation and click-chemistry. *Materials* 12(10):1580. <https://doi.org/10.3390/ma12101580>
- Mahmoodi NM, Hayati B, Arami M, Lan C (2011) Adsorption of textile dyes on Pine Cone from colored wastewater: kinetic, equilibrium and thermodynamic studies. *Desalination* 268(1–3):117–125. <https://doi.org/10.1016/j.desal.2010.10.007>
- Mashabi RA, Khan ZA, Elwakeel KZ (2022) Chitosan or glycidyl methacrylate-based adsorbents for dyes removal from the aqueous solutions: a brief review. *Mater Adv* 3(14):5645–5671. <https://doi.org/10.1039/d2ma00320a>
- Mashkoo F, Nasar A, Asiri AM (2018) Exploring the reusability of synthetically contaminated wastewater containing crystal violet dye using *tectona grandis* sawdust as a very low-cost adsorbent. *Sci Rep* 8(1):1–16. <https://doi.org/10.1038/s41598-018-26655-3>
- El Messaoudi N, El Khomri M, Chlif N, Chegini ZG, Dbik A, Bentahar S, Lacherai A (2021) Desorption of Congo red from dye-loaded *Phoenix dactylifera* date stones and *Ziziphus lotus* jujube shells. *Groundw Sustain Dev* 12:100552. <https://doi.org/10.1016/j.gsd.2021.100552>
- Mirza A, Ahmad R (2020) An efficient sequestration of toxic crystal violet dye from aqueous solution by Alginate/Pectin nanocomposite: a novel and ecofriendly adsorbent. *Groundw Sustain Dev* 11:200373. <https://doi.org/10.1016/J.GSD.2020.100373>
- Nordine N, El Bahri Z, Sehil H, Fertout RI, Rais Z, Bengharez Z (2016) Lead removal kinetics from synthetic effluents using Algerian pine, beech and fir sawdust's: optimization and adsorption mechanism. *App Water Sci* 6(4):349–358. <https://doi.org/10.1007/s13201-014-0233-3>
- Ogana FN, Corral-Rivas S, Gorgoso-Varela JJ (2020) Non-linear mixed-effect height-diameter model for *Pinus pinaster* ait. and *Pinus radiata* d. don. *Cerne* 26(1):150–161. <https://doi.org/10.1590/01047760202026012695>
- Orozco CI, Freire MS, Gómez-Díaz D, González-Álvarez J (2023) Removal of copper from aqueous solutions by biosorption onto pine sawdust. *Sustain Chem Pharm* 32:101016. <https://doi.org/10.1016/j.scp.2023.101016>
- Özacar M, Şengil IA (2005) Adsorption of metal complex dyes from aqueous solutions by pine sawdust. *Bioresour Technol* 96(7):791–795. <https://doi.org/10.1016/j.biortech.2004.07.011>
- Özdemir ÇS (2019) Equilibrium, kinetic, diffusion and thermodynamic applications for dye adsorption with pine cone. *Sep Sci Technol* 54(18):3046–3054. <https://doi.org/10.1080/01496395.2019.1565769>
- Philippou K, Anastopoulos I, Pashalidis I, Hosseini-Bandeharaei A, Usman M, Kornaros M, Omirou M, Kalderis D, Milojković JV, Lopičić ZR, Abatal M (2021) Chapter 6 - The application of pine-based adsorbents to remove potentially toxic elements from aqueous solutions. In: Núñez-Delgado A (ed) *Sorbents materials for controlling environmental pollution*. Elsevier, pp 113–133
- Ratnamala GM, Deshannavar UB, Munyal S, Tashildar K, Patil S, Shinde A (2016) Adsorption of reactive blue dye from aqueous solutions using sawdust as adsorbent: optimization, kinetic, and equilibrium studies. *Arab J Sci Eng* 41(2):333–344. <https://doi.org/10.1007/s13369-015-1666-1>
- Reijnga J, van Hoof A, van Loon A, Teunissen B (2013) Development of methods for the determination of pKa values. *Anal Chem Insights* 8(1):53–71. <https://doi.org/10.4137/ACI.S12304>
- Rouquerol J, Rouquerol F, Sing KSW, Llewellyn P, Maurin G (2014) *Adsorption by powders and porous solids: principles, methodology and applications*. Academic Press, London
- Sahmoune MN, Yeddou AR (2016) Potential of sawdust materials for the removal of dyes and heavy metals: examination of isotherms and kinetics. *Desalin Water Treat* 57(50):24019–24034. <https://doi.org/10.1080/19443994.2015.1135824>
- Salazar-Rabago JJ, Leyva-Ramos R, Rivera-Utrilla J, Ocampo-Perez R, Cerino-Cordova FJ (2017) Biosorption mechanism of Methylene Blue from aqueous solution onto White Pine (*Pinus durangensis*) sawdust: effect of operating conditions. *Sustain Environ Res* 27(1):32–40. <https://doi.org/10.1016/j.serj.2016.11.009>
- Schaffer M, Licha T (2014) A guideline for the identification of environmentally relevant, ionizable organic molecule species. *Chemosphere* 103:12–25. <https://doi.org/10.1016/j.chemosphere.2013.12.009>
- Semerjian L (2018) Removal of heavy metals (Cu, Pb) from aqueous solutions using pine (*Pinus halepensis*) sawdust: equilibrium, kinetic, and thermodynamic studies. *Environ Technol Innov* 12:91–103. <https://doi.org/10.1016/j.eti.2018.08.005>
- Şentürk I, Yıldız MR (2020) Highly efficient removal from aqueous solution by adsorption of Maxilon Red GRL dye using activated pine sawdust. *Korean J Chem Eng* 37(6):985–999. <https://doi.org/10.1007/s11814-020-0526-1>
- Sulyman M, Gierak A (2020) Green environmental approach for adsorption of hazardous dye from water using tree and sea plant leaves (Dead L.). *Acta Sci Agric* 4(2):1–10
- Weber WJ Jr, Morris JC (1963) Kinetics of adsorption on carbon from solution. *J Sanit Eng Div* 89(2):31–59
- Zafar S, Akhtar S, Tariq T, Mushtaq N, Akram A, Ahmed A, Arif M, Naeem S, Anwar S (2014) Determination of pKa values of new phenacyl-piperidine derivatives by potentiometric titration method in aqueous medium at room temperature (25±0.5°C). *Pak J Pharm Sci* 27:925–929

Publisher's Note Springer Nature remains neutral with regard to jurisdictional claims in published maps and institutional affiliations.